Ch. 8 in L. H. Wang (Editor) "Photoacoustic imaging and spectroscopy," CRC Press 2009, pp. 89-101.

8 On Reconstruction Formulas and Algorithms for the Thermoacoustic Tomography

Mark Agranovsky
Bar-Ilan University

Peter Kuchment
Texas A&M University

Leonid Kunyansky
University of Arizona

CONTENTS

8.1 Introduction 89
8.2 Thermoacoustic Tomography 90
8.3 Mathematical Model of TAT 90
8.4 Uniqueness of Reconstruction 91
8.5 Reconstruction in the Case of Constant Sound Speed: Formulas, Algorithms, and Examples 92
8.5.1 Inversion Formulas and Procedures 92
8.5.1.1 Approximate Inversion Formulas 92
8.5.1.2 Exact Filtered Backprojection Formulas in 3D 92
8.5.1.3 Exact Filtered Backprojection Formulas in 2D 93
8.5.2 Series Solutions for Arbitrary Geometries 95
8.6 Reconstruction in the Case of Variable Sound Speed 95
8.7 Partial Data.Visible and Invisible Singularities 96
8.8 Range Conditions 96
8.9 Concluding Remarks 98
8.9.1 Uniqueness 98
8.9.2 Inversion 98
8.9.3 Stability 99
8.9.4 Range 99
Acknowledgments 99
References 99

8.1 INTRODUCTION

Recent years have brought about exciting new developments in computerized tomography. In particular, a novel, very promising approach to the creation of diagnostic techniques consists in combining different imaging modalities, in order to take advantage of their individual strengths. Perhaps the most successful example of such a combination is the thermoacoustic tomography (TAT) (also called photoacoustic tomography and optoacoustic tomography and abbreviated as TCT, PAT, or OAT) [1–8].

Major progress has been made recently in developing the mathematical foundations of TAT, including proving uniqueness of reconstruction, obtaining range descriptions for the relevant operators, deriving inversion formulas and algorithms, understanding solutions of incomplete data problems, stability of solutions, etc. One can find a survey of these results and extensive bibliography in Ref. [9]. In the present article, we concentrate on the recent advances in the inversion formulas and algorithms for TAT. Mathematical problems of the same type arise also in sonar, radar, and geophysics

applications (e.g., Refs. [10–12]). Discussion of some mathematical problems concerning TAT can also be found in the chapters written by D. Finch and Rakesh and by S. Patch.

While this text addresses the mathematics of TAT only, one can find extensive discussion of physics, engineering, and biological issues related to TAT in the recent surveys [4,5,8], textbook [7], as well as in other chapters of this volume.

8.2 THERMOACOUSTIC TOMOGRAPHY

First, we give a brief description of TAT. The data acquisition starts with a short electromagnetic (EM) pulse being sent through the biological object under investigation (e.g., woman's breast in mammography).* A fraction of EM energy is absorbed at each location x inside the object, thus triggering thermoelastic expansion of the tissue and emergence of a pressure wave $p(x, t)$ (an ultrasound signal) that, in turn, is measured by transducers placed along some *observation surface* S surrounding (completely or partially) the object (Figure 8.1). The initial pressure $p_0(x)=p(x,0)$ is determined by the intensity of the EM pulse (assumed to be known) and by the local properties of the tissue. It is known (e.g., Refs. [1,4,5,8,13]) that in the radiofrequency and visible light ranges, absorption of the EM energy by cancerous cells is several times stronger than by the healthy ones. Thus, knowledge of the initial pressure $p_0(x)$ would provide an efficient tool for early detection of cancer. Frequently, the ultrasound contrast is sufficiently small to justify the use of the constant sound speed approximation. To date, most work on TAT is based on this assumption. However, such an approximation is not always appropriate; some of the results described below, as well as in Refs. [9,14,15] aim towards the general case of a variable speed of sound.

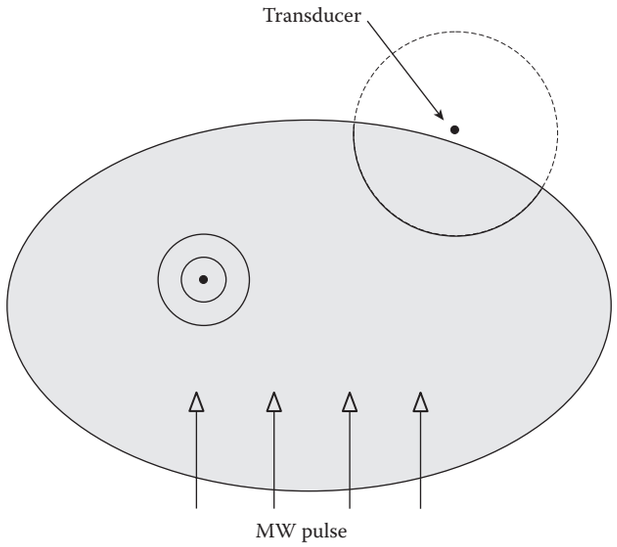

FIGURE 8.1 The TAT procedure. (Reproduced from Kuchment, P., and L. Kunyansky, *Eur. J. Appl. Math.* 19(2):191–224, 2008. With permission.)

Once the data $p(x, t)$ has been measured on $S \times \mathbb{R}^+$, one can attempt to recover from $p(x, t)$ the initial value $p_0(x)$ of the pressure inside S (the thermoacoustic image).

8.3 MATHEMATICAL MODEL OF TAT

Let us for notational convenience denote $p_0(x)$ (the image to be reconstructed) by $f(x)$. In this section, we present a mathematical description of the relation between the functions $f(x)$ and $p(x, t)$. We assume that the function $f(x)$ is compactly supported in $\mathbb{R}^n$ (we allow the dimension to be arbitrary, albeit the most interesting cases for TAT are $n = 3$ and $n = 2$). At each point y of an observation surface S one places a point detector** that measures the value of the pressure $p(y, t)$ at any moment $t>0$. It is usually assumed that the surface S is closed (rather than, say, a cylinder or a plane***). It is also assumed that the object (and thus the support of $f(x)$) is completely surrounded by S. The latter assumption is crucial for the validity of most inversion formulas; however, in some cases we will be able to abandon this requirement.

The mathematical model described below relies upon some physical assumptions on the measurement process, which we will not describe here. The reader can find such a discussion in Ref. [8].

We assume that the ultrasound speed $v_s(x)$ is known, e.g., through transmission ultrasound measurements [15]. Then, the pressure wave $p(x, t)$ satisfies the following set of equations [13,23,24]:

$$\begin{cases} p_{tt} = v_s^2(x)\Delta_x p, & t \geq 0 \quad x \in \mathbb{R}^n \\ p(x,0) = f(x), \\ p_t(x,0) = 0 \end{cases} . \tag{8.1}$$

Now one needs to recover the initial value $f(x)$ at $t=0$ of the solution $p(x,t)$ from the measured data $g(y,t) := p(y,t), y \in S, t \geq 0$. Incorporating this data, one rewrites Equation 8.1 as

$$\begin{cases} p_{tt} = v_s^2(x)\Delta_x p, & t \geq 0, \quad x \in \mathbb{R}^n \\ p(x,0) = f(x), \\ p_t(x,0) = 0 \\ p(y,t) = g(y,t), & y \in S \times \mathbb{R}^+ \end{cases} . \tag{8.2}$$

In other words, we would like to recover the initial value $f(x)$ in Equation 8.2 from the knowledge of the lateral data $g(y, t)$ (see Figure 8.2). At first glance, it seems that the data is insufficient for the reconstruction, i.e., for recovering the solution of the wave equation in a cylinder from the lateral values alone. However, this impression is incorrect, since there is additional information that the solution holds in the whole space, not just

* It has been argued that the radiofrequency and visible light ranges are most appropriate in TAT [8]. For the purpose of this text, no distinction is made between these cases.

** Planar and linear detectors have been considered as well, see Refs. [16, 17] and further references in Ref. [9].

***Reconstruction formulas for the planar and cylindrical cases are well known, see, e.g., Refs. [18–22].

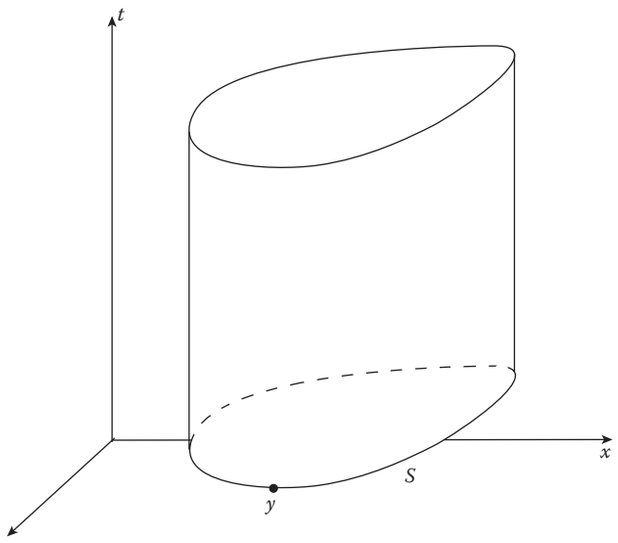

FIGURE 8.2 An illustration to Equation 8.2. (Reproduced from Kuchment, P., and L. Kunyansky, *Eur. J. Appl. Math.* 19(2):191–224, 2008. With permission.)

inside the cylinder $S\times\mathbb{R}^+$. To put it differently, if one solves not only the internal, but also the external problem for the wave equation with the data g on the cylinder $S\times\mathbb{R}^+$, then the solutions must have matching normal derivatives on $S\times\mathbb{R}^+$. In most cases, this additional information provides uniqueness of recovery of $f(x)$ (see below, as well as Refs. [9,14,25–29] and references therein). It is also sometimes useful to notice that p can be extended as an even function of time and thus satisfies the wave equation for all values of t. Similarly, data g can be extended to an even function. This, in particular, enables one to apply Fourier transform in time.

An additional structure arises in this problem, if one assumes that the object under investigation is nearly homogeneous with respect to ultrasound: $\nu_s(x)=1$. In this constant speed case, there is an alternative way to describe the relation between the data $g(y,t)\in S\times\mathbb{R}^+$ and the unknown image $f(x)$, $x\in\mathbb{R}^3$. The known Poisson–Kirchhoff formulas (see Ref. [30] Chapter VI, Section 13.2, Formula (15)) for the solution of Equation 8.1 with $\nu_s=1$ give

$$p(x,t)=\frac{\partial}{\partial t}\big(t(Rf)(x,t)\big), \tag{8.3}$$

where

$$(Rf)(x,r)=\frac{1}{4\pi}\int_{|y|=1} f(x+ry)dA(y), \tag{8.4}$$

is the *spherical mean operator* applied to the function $f(x)$, and dA is the surface area element on the unit sphere in $\mathbb{R}^3$. Thus, the function $g(y,t)$ for $y\in S$ and all $t\geq 0$ essentially carries the same information as the spherical mean $Rf(y,t)$ at all points $(y,t)\in S\times\mathbb{R}^+$ (see, e.g., Ref. [27]). One can, therefore, study the spherical mean operator $R: f\to Rf$ and, in particular, its restriction R_S to the points $y\in S$ of the observation surface:

$$R_S f(x,t)=\int_{|y|=1} f(x+ty)dA(y),\quad x\in S,\quad t\geq 0. \tag{8.5}$$

This explains why in many studies on TAT, the spherical mean operator has been used as the model. One needs to notice, though, that in the case of a nonconstant sound speed, the spherical mean interpretation (as well as any integral geometry approximation) is no longer valid, while the wave equation model still is.

8.4 UNIQUENESS OF RECONSTRUCTION

Uniqueness of reconstruction of a compactly supported (or sufficiently fast decaying) function $f(x)$ from the data g collected from a closed surface S is well known in the case of a constant sound speed (i.e., when the interpretation in terms of spherical mean operators is possible). One can find discussion of such results in Refs. [9,14,25,27–29,31–34].

In the case of a variable sound speed, it is shown in Ref. [31, Theorem 4] that uniqueness of reconstruction also holds for a smoothly varying (positive) sound speed, if the function $f(x)$ is supported inside the observation surface S. The proof uses the famous unique continuation theorem by D. Tataru [35].

We now present a recent simple uniqueness theorem that also allows a nonconstant sound speed $\nu_s(x)$ and does not require the function to be supported inside S. In order to do so, first we need to formulate some assumptions on $\nu_s(x)$ and the function $f(x)$ to be reconstructed.

1. Support of $f(x)\in H^s_{\rm loc}(\mathbb{R}^n)$, $s>1/2$ is compact.
2. The sound speed is smooth (a condition that can be reduced), strictly positive $\nu_s(x)>\nu_0>0$, and such that $\nu_s(x)-1$ has compact support, i.e., $\nu_s(x)=1$ for large x.
3. Consider the Hamiltonian system in $\mathbb{R}^{2n}_{x,\xi}$ with the Hamiltonian $H=((\nu_s^2(x))/2)|\xi|^2$:

$$\begin{cases} x_t'=\dfrac{\partial H}{\partial \xi}=\nu_s^2(x)\xi \\ \xi_t'=-\dfrac{\partial H}{\partial x}=-\dfrac{1}{2}\nabla(\nu_s^2(x))\,|\,\xi\,|^2. \\ x\,|_{t=0}=x_0,\quad \xi\,|_{t=0}=\xi_0. \end{cases} \tag{8.6}$$

The solutions of this system are called *bicharacteristics* and their projections into $\mathbb{R}^n_x$ are *rays*.
We will assume that the **nontrapping condition** holds, i.e., that all rays (with $\xi_0\neq 0$) tend to infinity when $t\to\infty$.

Theorem 1. [14] *Under the assumptions formulated above, compactly supported function $f(x)$ is uniquely determined by*

the data g. (*No assumption of f being supported inside S is imposed.*)

Uniqueness fails, however, if *f* does not decay sufficiently fast (see Ref. [25], where it is shown for the constant speed in which spaces $L^p(\mathbb{R}^d)$ of functions $f(x)$ closed surfaces remain uniqueness sets).

8.5 RECONSTRUCTION IN THE CASE OF CONSTANT SOUND SPEED: FORMULAS, ALGORITHMS, AND EXAMPLES

We consider here the case of a constant sound speed: $v_s(x)=1$. Then, one can work either with the wave equation or with the spherical mean operator model.

8.5.1 Inversion Formulas and Procedures

Consider the case of the observation surface *S* being a sphere. The first inversion procedures for this situation were obtained in Ref. [36] in 2D and in Ref. [37] in 3D by harmonic decomposition of the measured data *g* and of the function *f*, and then by equating coefficients of the corresponding Fourier series (see also Ref. [9] for a brief description of this procedure). The two resulting series solutions are not quite analogous. Indeed, in Ref. [36], one had to divide the Hankel transform of the data by the Bessel functions that have infinitely many zeros, which would create instabilities during implementation. The 3D solution in Ref. [37] is free of this difficulty and can also be adopted for 2D. We will see a different type of series solutions later on in this section.

8.5.1.1 Approximate Inversion Formulas

The standard way of inverting Radon transform in tomographic applications is by using filtered backprojection-type formulas [20,38–41]. It combines a linear filtration of projections (either in Fourier domain, or by a convolution with a certain kernel) followed (or preceded) by a backprojection. In the case of the set of spheres centered on a closed surface (e.g., sphere) *S*, one expects such a formula to involve a filtration with respect to the radial variable and an integration over the set of spheres passing through the point *x* of interest. Albeit for quite a long time no such formula had been discovered, this did not prevent practitioners from reconstructions. The reason was that good approximate inversion formulas (parametrices) could be developed, followed by an optional iterative improvement of the reconstruction [6,13,21,22,42–44]. Perhaps the most advanced approach of this kind was adopted by Popov and Sushko [42,43]. These authors have developed a set of "straightening" formulas that allow one to reconstruct from the spherical means an approximation to the regular Radon projections. The main idea is that for each (hyper)plane passing through the support of the function to be reconstructed, one builds a family of spheres with centers at the detectors' locations and tangential to that plane. One such sphere is chosen for each point of the plane contained within the support. The integrals over these spheres are known, as they form a subset of projections *g*. An approximation to the integral of the function over the plane is then computed by integrating over these projections a functional (local in odd and nonlocal in even dimensions). When all the plane integrals are computed, the function is reconstructed by applying inversion formulas for the regular Radon transform. This procedure is not exact; however, as shown in Ref. [42], such an algorithm yields a parametrix. Namely, the difference between such an approximation and the original function *f* is described by a pseudodifferential operator of order −1 applied to *f*. In other words, reconstruction is accurate up to a smoothing operator. This result holds even if the measuring surface is not closed (but satisfies a "visibility" condition), which is important for applications in the problems with incomplete data.

8.5.1.2 Exact Filtered Backprojection Formulas in 3D

The first set of exact inversion formulas of the filtered backprojection-type for the spherical surface *S* was discovered in Ref. [29]. These formulas were obtained only in odd dimensions (and then extended to even dimensions in Ref. [45]). Various versions of such formulas (different in terms of the order in which the filtration and backprojection steps are performed) were developed.

To describe these formulas, let us assume that *B* is the unit ball, $S=\partial B$ is the unit sphere in $\mathbb{R}^3$, and a function $f(x)$ is supported inside *S*. The values of its spherical integrals $g(z,r)$ with the centers on *S* are assumed to be known:

$$g(z,r)=\int_{S^2} f(z+rs)r^2 dA(s) = 4\pi r^2 R_S f(z,r), \quad z\in S. \quad (8.7)$$

Some of the 3D inversion formulas of Ref. [29] are:

$$f(y) = -\frac{1}{8\pi^2}\Delta_y \int_S \frac{g\left(z,\left|z-y\right|\right)}{\left(\left|z-y\right|\right)} dA(z), \quad (8.8)$$

$$f(y) = -\frac{1}{8\pi^2}\int_S \left(\frac{1}{t}\frac{d^2}{dt^2} g(z,t)\right)\Bigg|_{t=|z-y|} dA(z). \quad (8.9)$$

A different set of explicit inversion formulas, which work in arbitrary dimensions, was found in Ref. [46]. In 3D case, the general expression derived in Ref. [46] simplifies to

$$f(y) = \frac{1}{8\pi^2}\,\mathrm{div}\int_S n(z)\left(\frac{1}{t}\frac{d}{dt}\frac{g(z,t)}{t}\right)\Bigg|_{t=|z-y|} dA(z), \quad (8.10)$$

where $n(z)$ is the vector of exterior normal to *S*. (In this expression, we eliminated the minus sign erroneously present in the original formula.) Equation 8.10 is equivalent to one of the 3D formulas derived earlier in Ref. [47].

Similar to the case of the standard "flat" Radon transform, all these 3D inversion formulas are local, i.e., in order to reconstruct a value of the function at a certain point, one needs to know only the values of all the integrals over the spheres passing through an infinitesimally small neighborhood of that point.

should be "belong"

It is worth noting that although Formulas 8.9 and 8.10 yield identical results when applied to functions that belongs to the range of the spherical mean Radon transform, they are, in general, not equivalent, i.e., lead to different reconstructions when the data is outside of the range (for instance, due to errors). Another important fact about these reconstruction techniques is that, unfortunately, they do not yield correct reconstruction within the region surrounded by the detectors if the source is not contained within this region. Both these statements can be easily proven by the following example. Let us assume that the source function $f(x)$ is constant (equal to 1) within the ball $B(0,3)$ of radius 3 centered at the origin. In order to reconstruct the function within the unit ball, Formulas 8.10 and 8.9 use only integrals over spheres with the radius less or equal to 2, and centered at the points of the unit sphere. Obviously, all these spheres lie within the $B(0,3)$, and thus the projections $g(z,t)$ are equal to the areas of the corresponding integration spheres, i.e., to $4\pi t^2$. By substituting this expression into Equation 8.9, we obtain

$$f_1(y) = -\frac{1}{\pi R}\int_S \frac{1}{|z-y|}\,dA(z).$$

Function $f_1(y)$ defined by the above formula is harmonic in the interior of B, since the integrand is the free space Green's function of the Laplace equation. Due to the symmetry of the geometry, $f_1(y)$ is radially symmetric, i.e., it depends only on $|y|$. Therefore, $f_1(y)=\text{const}$ for all $y\in B\backslash S$. Let us compute $f_1=0$:

$$f_1(0) = -\frac{1}{\pi R}\int_S \frac{1}{R}\,dA(z) = -4.$$

Thus, $f_1(y)=-4$ for all $y\in B\backslash S$.

A similar computation with the use of Equation 8.10 yields

$$f_2(y) = \frac{1}{2\pi}\,\mathrm{div}\int_S n(z)\frac{1}{|z-y|}\,dA(z)$$
$$= -\frac{1}{2\pi}\int_S \frac{d}{dn(z)}\frac{1}{|z-y|}\,dA(z) = \frac{4\pi}{2\pi} = 2,$$

where we used the 3D Gauss formula. Both results f_1 and f_2 are incorrect (not equal to 1). Besides, they are different, which proves that Formulas 8.9 and 8.10 are not equivalent.

One of the important benefits of having exact inversion formulas is that often a rather straightforward discretization of such a formula yields an efficient and stable reconstruction algorithm. Such algorithms were developed in Ref. [48] using Equations 8.8 and 8.9, and in Ref. [46] utilizing Formula 8.10.

In the simplest case, when the image is reconstructed on a grid of size $m\times m\times m$ from $\mathcal{O}(m^2)$ projections, each of which contains values for $\mathcal{O}(m)$ integration spheres, all these algorithms have complexity of $\mathcal{O}(m^5)$ operations. In practical terms, for m of order of a hundred, the reconstruction time is measured in hours. An example of the reconstruction in 3D using a method based on Formula 8.10, is shown in Figure 8.3. Reconstructions using Formulas 8.8 or 8.9 are quite similar in terms of stability, accuracy, and computation time.

8.5.1.3 Exact Filtered Backprojection Formulas in 2D

Exact inversion formulas were obtained for even dimensions in Ref. [45]. Denoting by g, as before, the spherical integrals (rather than averages) of f, the formulas in 2D look as follows:

$$f(y) = \frac{1}{4\pi^2 R}\Delta\int_S\int_0^{2R} g(z,t)\log\left|t^2-|y-z|^2\right|dt\,dl(z), \qquad (8.11)$$

or

$$f(y) = \frac{1}{4\pi^2 R}\int_S\int_0^{2R}\frac{\partial}{\partial t}\left(t\frac{\partial}{\partial t}\frac{g(z,t)}{t}\right)$$
$$\times\log\left|t^2-|y-z|^2\right|dt\,dl(z), \qquad (8.12)$$

where B is a disk of radius R centered at the origin, and $S=\partial B$ is its boundary.

Another 2D inversion formula [46] takes the following form (again, corrected for a sign):

$$f(y) = -\frac{1}{8\pi}\,\mathrm{div}\int_S n(z)h\left(z,|y-z|\right)dl(z), \qquad (8.13)$$

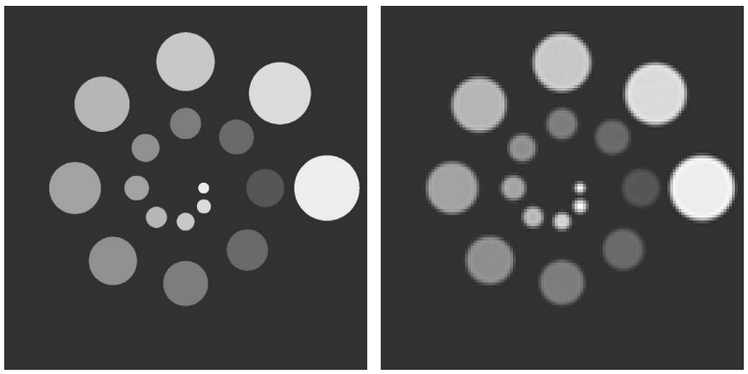

FIGURE 8.3 A mathematical phantom in 3D (left) and its reconstruction using inversion Formula 8.10.

where

$$h(z,t)=\int_{\mathbb{R}^+}\left[Y_0(\lambda t)\left(\int_0^{2R}J_0(\lambda t')g(z,t')dt'\right)-J_0(\lambda t)\left(\int_0^{2R}Y_0(\lambda t')g(z,t')dt'\right)\right]\lambda d\lambda, \quad (8.14)$$

and $J_0(t)$ and $Y_0(t)$ are the Bessel and Neumann functions of order 0. By analyzing the large argument asymptotics of these functions, one can see [46] that the filtration operator given by Equation 8.14 is an analog of the Hilbert transform.

This reconstruction procedure can be rewritten in a form similar to Equations 8.11 or 8.12. Indeed, by slightly modifying the original derivation of Equations 8.13 and 8.14, one can obtain a formula that would reconstruct a smoothed version $\hat{f}(x, \nu)$ of $f(x)$ defined by the formula

$$\hat{f}(x,\nu)=\mathcal{F}^{-1}\left(|\xi|^{-\nu}\mathcal{F}f\right), \quad 0<\nu<1,$$

where $\mathcal{F}$, $\mathcal{F}^{-1}$ are correspondingly the 2D Fourier and inverse Fourier transforms. The restriction of $\hat{f}(x, \nu)$ to the interior of the disk B is recovered by the formula

$$\hat{f}(y,\nu)=-\frac{1}{8\pi}\operatorname{div}\int_S n(z)h_\nu\left(z,|y-z|\right)dl(z), \quad (8.15)$$

where

$$h_\nu(z,t)=\int_{\mathbb{R}^+}Y_0(\lambda t)\left(\int_0^{2R}J_0(\lambda t')g(z,t')dt'\right)-J_0(\lambda t)\left(\int_0^{2R}Y_0(\lambda t')g(z,t')dt'\right)\lambda^{-\nu}d\lambda. \quad (8.16)$$

For $0 < v < 1$, one can change the order of integration in Equation 8.16 to obtain

$$h_\nu(z,t)=\int_0^{2R}g(z,t')K_\nu(z,t,t')dt', \quad (8.17)$$

$$K_\nu(z,t,t')=\int_{\mathbb{R}^+}Y_0(\lambda t)J_0(\lambda t')\lambda^{-\nu}d\lambda-\int_{\mathbb{R}^+}J_0(\lambda t)Y_0(\lambda t')\lambda^{-\nu}d\lambda. \quad (8.18)$$

Using Ref. [49, Formula 4.5, p. 211], the integral $\int_{\mathbb{R}^+}Y_0(\lambda t)J_0(\lambda t')\lambda^{-\nu}d\lambda$ can be evaluated exactly, yielding

$$\int_{\mathbb{R}^+}Y_0(\lambda t)J_0(\lambda t')\lambda^{-\nu}d\lambda=\begin{cases}\dfrac{2^{1-\nu}}{\pi}\Gamma(1-\nu)\dfrac{t^{-\nu}\cos(\pi\nu)}{\left|t^2-t'^2\right|^{1-\nu}}, & t>t'\\ -\dfrac{2^{1-\nu}}{\pi}\Gamma(1-\nu)\dfrac{t^{-\nu}}{\left|t^2-t'^2\right|^{1-\nu}}, & t<t'\end{cases}.$$

The expression for the second integral in Equation 8.18 is derived by interchanging t and t', which results in the formula

$$K_\nu(z,t,t')=\begin{cases}\dfrac{2^{1-\nu}}{\pi}\Gamma(1-\nu)\dfrac{t^{-\nu}\cos(\pi\nu)+(t')^{-\nu}}{\left|t^2-t'^2\right|^{1-\nu}}, & t>t'\\ -\dfrac{2^{1-\nu}}{\pi}\Gamma(1-\nu)\dfrac{(t')^{-\nu}\cos(\pi\nu)+t^{-\nu}}{\left|t^2-t'^2\right|^{1-\nu}}, & t<t'\end{cases}.$$

Finally, we substitute the above expression for $K_\nu(z, t, t')$ into Equation 8.17 and take the limit $\nu \to 0$, to arrive at the following formulas

$$f(y)=\frac{1}{2\pi^2}\operatorname{div}\int_S n(z)h_0\left(z,|y-z|\right)dl(z),$$

$$h_0(z,t)=\int_0^{2R}g(z,t')\frac{1}{t'^2-t^2}dt',$$

or

$$f(y)=\frac{1}{2\pi^2}\operatorname{div}\int_S n(z)\left[\int_0^{2R}g(z,t')\frac{1}{t'^2-|y-z|^2}dt'\right]dl(z). \quad (8.19)$$

Similar to the one appearing in Equations 8.11 and 8.12, the filtration operator in Equation 8.19 also involves kernel $1/(t'^2-t^2)$. If desired, it can be rewritten in the form of a convolution, either by the change of variables $t^2 \to t$, or by noticing that

$$\frac{2}{t'^2-t^2}=\frac{1/t'}{t+t'}-\frac{1/t'}{t-t'}.$$

This is important from the computational point of view, since it allows the reduction of the inner integral in Equation 8.19 to the sum of two Hilbert transforms, computational algorithms for which are well known.

All inversion formulas presented in this section require $\mathcal{O}(m^3)$ operations to reconstruct an image on a grid of size $m \times m$ from $\mathcal{O}(m)$ projections, each consisting of $\mathcal{O}(m)$ values of circular integrals. This coincides with the operation count required by a classical (nonaccelerated) filtered backprojection algorithm in 2D.

Currently, it is not known whether Formula 8.19 is equivalent to Equations 8.11 and 8.12. However, as shown in the previous section, this is not the case for the 3D versions of these formulas, and thus this seems unlikely in the two-dimensional case as well.

Finally, similar to the filtered backprojection formulas for the classical 2D Radon transform, the inversion Formulas 8.11, 8.12, and 8.19 are not local. In other words, in order to recover the value of $f(x)$ for a fixed point x, all the values of $g(z, t)$ have to be known.

8.5.2 Series Solutions for Arbitrary Geometries

Explicit inversion formulas for closed surfaces S different from spheres have not yet been found,[§] except the result of Ref. [14] described in the next section. There is, however, a different approach [50] that theoretically works for any closed S and that is practically useful when the surface is the boundary of a region, in which the spectrum and eigenfunctions of the Dirichlet Laplacian are known (or could be effectively approximated numerically).

Let λ_k^2 (where $\lambda_k > 0$) and $u_k(x)$ be the eigenvalues and normalized eigenfunctions of the Dirichlet Laplacian $-\Delta_D$ on the interior Ω of the observation surface S:

$$\begin{aligned} \Delta u_k(x) + \lambda_k^2 u_k(x) = 0, \quad x \in \Omega, \quad \Omega \subseteq \mathbb{R}^n, \\ u_k(x) = 0, \quad x \in S = \partial\Omega, \\ \|u_k\|_2^2 \equiv \int_\Omega |u_k(x)|^2 \, dx = 1. \end{aligned} \tag{8.20}$$

As before, we would like to reconstruct a compactly supported function $f(x)$ from the known values of its spherical integrals $g(z, r)$ (Equation 8.7).

According to Ref. [50], if $f(x)$ is represented as the sum of the Fourier series

$$f(x) = \sum_{m=0}^{\infty} \alpha_k u_k(x), \tag{8.21}$$

the Fourier coefficients α_k can be reconstructed as follows:

$$\alpha_k = \int_{\partial\Omega} I(z, \lambda_k) \frac{\partial}{\partial n} u_k(z) dA(z), \tag{8.22}$$

where

$$I(z, \lambda_k) = \int_{\mathbb{R}^+} g(z, r) \Phi_{\lambda_k}(r) dr,$$

and $\Phi_{\lambda_k}(|x-z|)$ is a free-space rotationally invariant Green's function of the Helmholtz Equation 8.20.

Formula 8.22 is obtained by substituting the Helmholtz representation for $u_k(x)$

$$u_k(x) = \int_{\partial\Omega} \Phi_{\lambda_k}\left(|x-z|\right) \frac{\partial}{\partial n} u_k(z) ds(z) \quad x \in \Omega, \tag{8.23}$$

into the expression for the projections $g(z,t)$.

This eigenfunction expansion approach requires knowledge of the spectrum and eigenfunctions of the Dirichlet Laplacian, which is available only for some simple domains. However, when this information is available, the method yields reliable, robust, and, in some cases, fast reconstruction. For example, as it was shown in Ref. [50], for the cubic observation surface S, one can compute reconstructions thousands of times faster than by methods based on explicit inversion formulas of backprojection type discussed above. The operation count for such an algorithm is $\mathcal{O}(m^3 \log m)$, as compared to $\mathcal{O}(m^5)$ for the explicit inversion formulas.

Another advantage of the series technique is its ability to "tune out" the signal coming from outside of S. In other words, unlike the explicit inversion formulas discussed in the previous sections, the present method enables one to reconstruct the values of $f(x)$ for all x lying inside S even in the presence of the sources outside. We illustrate this property by the reconstruction shown in Figure 8.4. (The dashed line in the left figure represents surface S, i.e., the location of the detectors.)

[§] Planar and cylindrical observation surfaces, for which such formulas are known [18–22], are not closed.

8.6 RECONSTRUCTION IN THE CASE OF VARIABLE SOUND SPEED

In this section, we consider a more general case of the variable sound speed $\nu_s(x)$. Our analysis is valid under previously imposed conditions on this speed, namely, that $\nu_s(x)$ is sufficiently smooth, strictly positive, nontrapping, and $\nu_s(x)-1$ is compactly supported.

Consider the Hilbert space $H = L^2(\Omega, \nu_s^{-2}(x)dx)$, i.e., the weighted L^2 space with the weight $\nu_s^{-2}(x)$. In this space, the naturally defined operator

$$A = -\nu_s^2(x)\Delta$$

in Ω with zero Dirichlet conditions on S is self-adjoint, positive, and has discrete spectrum $\{\lambda_k^2\}$ ($\lambda_k > 0$) with eigenfunctions $\psi_k(x) \in H$.

We also denote by E the operator of harmonic extension of functions from S to Ω. For example, for a function ϕ on S, the function $E\phi$ is harmonic inside Ω and coincides with ϕ on S.

Since we are dealing with the unobstructed wave propagation in the whole space (the surface S is not truly a boundary, but just an observation surface), and since we assumed that the sound speed is nontrapping and constant at infinity, the local energy decay type estimates of Refs. [51,52] (see also Ref. [53, Theorem 2.104]) apply. They also lead to the following reconstruction procedures:

Theorem 2. [14]

1. *The function $f(x)$ in Equation 8.2 can be reconstructed inside Ω as follows:*

$$f(x) = \left(E\, g\big|_{t=0}\right) - \int_0^\infty A^{-1/2} \sin(\tau A^{1/2}) E(g_{tt})(x, \tau) d\tau. \tag{8.24}$$

2. *Function $f(x)$ can be reconstructed inside Ω from the data g in Equation 8.2, as the following $L^2(\Omega)$-convergent series*:

$$f(x) = \sum_k f_k \psi_k(x), \tag{8.25}$$

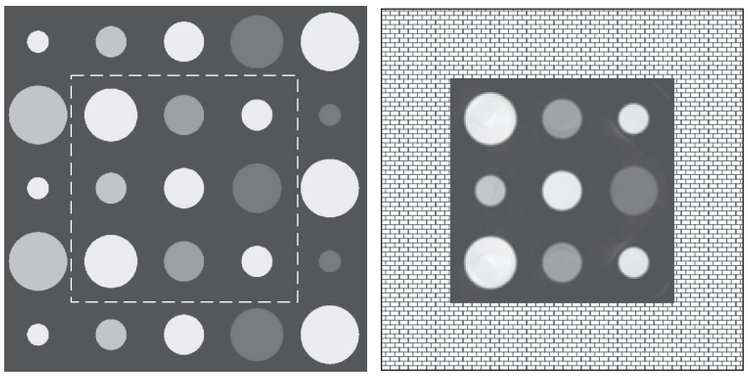

FIGURE 8.4 The phantom shown on the left includes several balls located outside the square acquisition surface S, which does not influence the reconstruction inside S (right).

where the Fourier coefficients f_k can be recovered using one of the following formulas:

$$\begin{cases} f_k = \lambda_k^{-2} g_k(0) - \lambda_k^{-3} \int_0^\infty \sin(\lambda_k t) g_k''(t)\,dt, \\ f_k = \lambda_k^{-2} g_k(0) + \lambda_k^{-2} \int_0^\infty \cos(\lambda_k t) g_k'(t)\,dt, \text{ or} \\ f_k = -\lambda_k^{-1} \int_0^\infty \sin(\lambda_k t) g_k(t)\,dt = -\lambda_k^{-1} \int_0^\infty \int_S \sin(\lambda_k t) \\ \quad \times g(x,t) \overline{\frac{\partial \psi_k}{\partial n}(x)}\,dx\,dt, \end{cases} \tag{8.26}$$

where

$$g_k(t) = \int_S g(x,t) \overline{\frac{\partial \psi_k}{\partial n}(x)}\,dx,$$

and n denotes the external normal to S.

Remark 3. *The function $E(g_{tt})$ does not belong to the domain of the operator A. The formula 8.24, however, still makes sense, since the operator $A^{-1/2} \sin(\tau A^{1/2})$ is bounded in L^2.*

This theorem in the particular case of the constant sound speed, implies the eigenfunction expansion procedure of Ref. [50] described in the previous section. However, unlike Ref. [50], it also applies to the variable speed situation and it does not require knowledge of a whole space Green's function. Similar to the method of Ref. [50] discussed in the preceding section, this procedure yields correct reconstruction inside the domain, even if a part of the source lies outside.

8.7 PARTIAL DATA. "VISIBLE" AND "INVISIBLE" SINGULARITIES

One can find a more detailed discussion of this issue for TAT in Ref. [9,44] and in the chapter [6] in this volume. Here we provide only a brief summary.

Uniqueness of reconstruction does not necessarily mean the possibility of practical reconstruction, since the reconstruction procedure can sometimes be unstable. This is true, for instance, in problems of electrical impedance tomography, and in incomplete data problems of x-ray tomography and TAT [20,34,41,55].

Microlocal analysis done in Refs. [10,56] (see also Ref. [57]) shows which parts of the wave front of a function f can be recovered from its partial x-ray or TAT data (see also Ref. [44] for a practical discussion). We describe this result in an imprecise form (see Ref. [10] for precise formulation), restricted to the case of jump singularities (tissue interfaces) only.

According to Refs. [10,56], for such singularities a part of the interface is stably recoverable (dubbed "visible" or "audible"), if for each point of the interface there exists a sphere centered at S and tangent to the interface at this point. Otherwise, the interface will be blurred away (even if there is a uniqueness of reconstruction theorem). Indeed, if all spheres of integration are transversal to the interface, the integration smoothes the singularity, and thus reconstruction of this interface becomes unstable. Figure 8.5 shows an example of a reconstruction from incomplete spherical mean data. The simulated transducers in this experiment were located along a 180° circular arc (the left half of a large circle surrounding the squares). In this figure, the sides of the squares that are not touched tangentially by circles centered on S are noticeably blurred; any kind of deblurring technique would not be stable in this context.

8.8 RANGE CONDITIONS

This paper would not be complete without mentioning the intimate relationship of inversion problems with range conditions. Indeed, as it has already been mentioned, recovery of f from the data g is impossible, if considered as an inverse problem for the wave equation problem inside the cylinder $S \times \mathbb{R}^+$. The possibility of inversion depends upon the fact that the solution of the wave equation lives in the whole space, and S is just the observation surface, rather than a true boundary. In other words, the data $g(x, t)$ comes from a very small (infinite codimension) subspace in any natural function space on the lateral boundary $S \times \mathbb{R}^+$. Thus, range conditions must

should be "Chapter 6", without brackets.

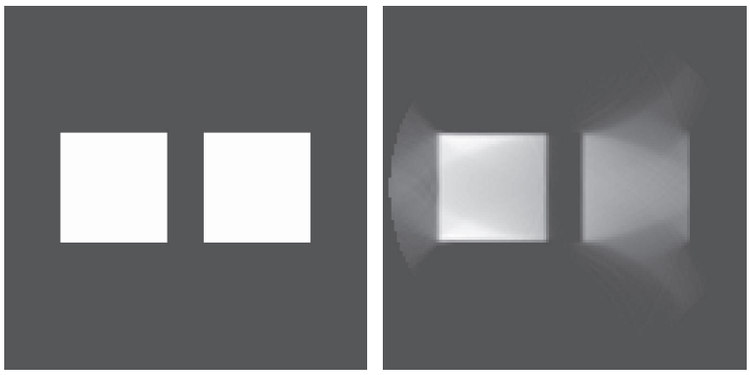

FIGURE 8.5 Effect of incomplete data: the phantom (left) and its reconstruction from incomplete data. (Reproduced from Kuchment, P., and L. Kunyansky, *Eur. J. Appl. Math.* 19(2):191–224, 2008. With permission.)

play a significant role. Indeed, they lead the authors of Ref. [14] to their results. We thus provide here a brief sketch of range results, following essentially the corresponding section of Ref. [9].

As has just been mentioned, the ranges of Radon-type transforms, including the spherical mean operator, are usually of infinite codimension in natural function spaces (in other words, ideal data should satisfy infinitely many consistency conditions). Information about the range is important for many theoretical and practical purposes (reconstruction algorithms, error corrections, incomplete data completion, etc.), and has attracted a lot of attention (e.g., Refs. [20,34,38–41,55,57–65]).

For example, functions g from the range of the standard Radon transform

$$f(x) \to g(s,\omega) = \int_{x\cdot\omega=s} f(x)dx, \; |\omega|=1,$$

satisfy two types of conditions:

1. *Evenness*: $g(-s,-\omega)=g(s,\omega)$
2. *Moment conditions*: for any integer $k\geq 0$, the kth moment

$$G_k(\omega) = \int_{-\infty}^{\infty} s^k g(\omega,s)ds$$

extends from the unit circle of vectors ω to a homogeneous polynomial of degree k in ω.

Although for the Radon transform the evenness condition seems to be "trivial", while the moment conditions seem to be the most important, this perception is misleading. Indeed, for more general transforms of Radon type it is often easier to find analogs of the moment conditions, while counterparts of the evenness conditions could be elusive (see Refs. [20,34,41,61,62,64]). This is exactly what happens with the spherical mean transform R_S.

An analog of the moment conditions was first presented implicitly in Refs. [27,66,67] and explicitly formulated as such in Refs. [68,69]:

Moment conditions *on data* $g(x,r)=R_Sf(x,r)$ *in* $\mathbb{R}^n$ *are: for any integer* $k\geq 0$*, the moment*

$$M_k(x) = \int_0^{\infty} r^{2k+n-1} g(x,r)dr, \quad x \in S$$

can be extended from S to a (*nonhomogeneous*) *polynomial* $Q_k(x)$ *of degree at most* $2k$.

These conditions are incomplete, and infinitely many others, which play the role of an analog of evenness, need to be added.

Complete range description for R_S when S is a sphere in 2D was found in Ref. [70] and then in odd dimensions in Ref. [71]. They were then extended to any dimension and provided several interpretations in Ref. [26]. These conditions, which happen to be intimately related to partial differential equations (PDEs) and spectral theory, are described below.

Let B be the unit ball in $\mathbb{R}^n$, $S=\partial B$ the unit sphere, and C the cylinder $B\times[0,2]$ (see Figure 8.6).

Consider the spherical mean operator R_S:

$$R_Sf(x,t)=G(x,t)=\int_{|y|=1} f(x+ty)dA(y).$$

If $G(x, t)$ is defined by the same formula for all $x \in \mathbb{R}^n$, then it satisfies the Darboux (Euler–Poisson–Darboux) equation [30,72,73]

$$G_{tt}+(n-1)t^{-1}G_t=\Delta_xG.$$

Inside the cylinder C, $G(x, t)$ vanishes when $t\geq 2$ (since the spheres of integration do not intersect the support of the function when $t\geq 2$).

Theorem 4. [26] *The following four statements are equivalent for any function* $g \in C_0^{\infty}(S\times[0,2])$*, where S is a sphere*:

1. *Function* g *is representable as* R_Sf *for some* $f \in C_0^{\infty}(B)$.
2. (*a*) *The moment conditions are satisfied.*
   (*b*) *The solution* $G(x, t)$ *of the interior Darboux problem satisfies the condition.*

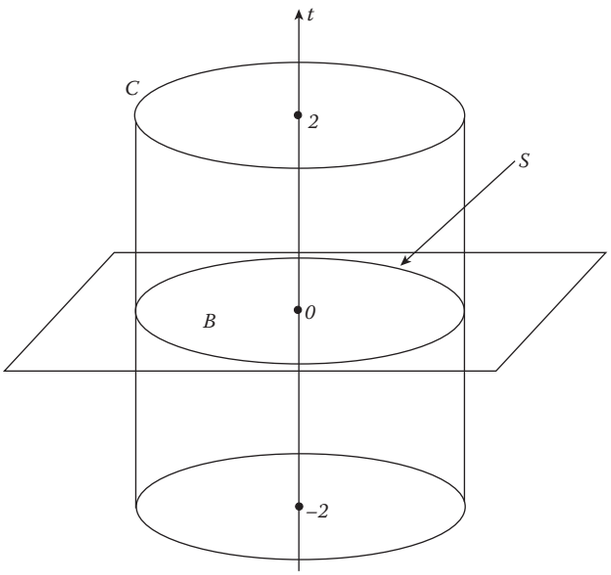

FIGURE 8.6 An illustration to the range description. (Reproduced from Kuchment, P., and L. Kunyansky, *Eur. J. Appl. Math.* 19(2):191–224, 2008. With permission.)

$$\lim_{t\to 0}\int_B \frac{\partial G}{\partial t}(x,t)\phi(x)dx = 0$$

for any eigenfunction $\phi(x)$ *of the Dirichlet Laplacian in B.*

3. (a) *The moment conditions are satisfied.*
   (b) *Let* $-\lambda^2$ *be an eigenvalue of Dirichle Laplacian in B and* ψ_λ *the corresponding eigenfunction. Then the following orthogonality condition is satisfied:*

$$\int_{S\times[0,2]} g(x,t)\partial_\nu \psi_\lambda(x) j_{n/2-1}(\lambda t)t^{n-1}dxdt = 0. \qquad (8.27)$$

Here $j_p(z) = c_p(J_p(z)/z^p)$ *is the so-called spherical Bessel function.*

4. (a) *The moment conditions are satisfied.*
   (b) *Let* $\hat{g}(x,\lambda) = \int g(x,t) j_{n/2-1}(\lambda t)t^{n-1}dt$. *Then, for any* $m\in\mathbb{Z}$, *the mth spherical harmonic term* $\hat{g}_m(x,\lambda)$ *of* $\hat{g}(x,\lambda)$ *vanishes at nonzero zeros of Bessel function* $J_{m+n/2-1}(\lambda)$.

One can make several important comments concerning this result (see Ref. [26] for a detailed discussion). In all of the remarks below, except the third one, the observation surface S is assumed to be a sphere.

1. If the dimension n is odd, then conditions (b) alone suffice for the complete range description, and thus they imply the moment conditions as well. (A similar earlier result was established for a related transform in Ref. [71].) It is not clear at the moment whether this holds true in even dimensions.
2. The range descriptions for R_S work in Sobolev scale, i.e., they describe the range of the operator $R_S : H^s_{\text{comp}}(B) \mapsto H^{s+(n-1)/2}_{\text{comp}}(S\times\mathbb{R}^+)$. (This uses a recent work by Palamodov [74]). Notice that in this result, it is assumed that the function f vanishes in a neighborhood of S, while in the previous theorem it was allowed for the support of f to reach all the way to the sphere S.
3. If S is not a sphere, but the boundary of a bounded domain, the range conditions 2 and 3 of the previous Theorem are still necessary for the data g to belong to the range of R_S. They, however, might no longer suffice for g to belong to the range.
4. A different wave equation approach to the range descriptions can be found in Ref. [71].

8.9 CONCLUDING REMARKS

8.9.1 Uniqueness

As already mentioned, the uniqueness questions relevant for TAT applications are essentially resolved. However, the mathematical understanding of the uniqueness problem for the restricted spherical mean operators R_S is still unsatisfactory and open-problems abound [9,27]. For instance, very little is known for the case of functions without compact support. The main known result is of Ref. [25], which describes for which values of $1\le p\le\infty$ the uniqueness result still holds:

Theorem 5. [25] *Let S be the boundary of a bounded domain in* $\mathbb{R}^n$ *and* $f\in L^p(\mathbb{R}^n)$ *such that* $R_S f\equiv 0$. *If* $p\le 2n/(n-1)$, *then* $f\equiv 0$ (*and thus S is the injectivity set for this space*). *This fails for any* $p>2n/(n-1)$.

The three- and higher-dimensional uniqueness problem for nonclosed observation surface S is also still open [9,27].

8.9.2 Inversion

Albeit closed-form (backprojection type) inversion formulas are available now for the cases of S being a plane (and object on one side from it), cylinder, and a sphere, there is still some mystery surrounding this issue. For instance, it would be interesting to understand whether (closed form, rather than series expansion) backprojection-type inversion formulas could be written for nonspherical observation surfaces S and/or in the presence of a nonuniform background $v_s(x)$. The results presented in Section 8.6 seem to be the first step in this direction.

Gelfand's

The I. Gelfand school of integral geometry has developed a powerful technique of the so-called κ operator, which provides a general approach to inversion and range descriptions for transforms of Radon type [39,58]. In particular, it has been applied to the case of integration over various collections ("complexes") of spheres in Refs. [39,75]. This consideration seems to suggest that one should not expect explicit closed-form inversion formulas for R_S when S is a sphere. However, such formulas were discovered in Refs. [29,45,46].

This apparent controversy (still short of contradiction) has not yet been resolved completely.

B. Rubin has recently discovered an alternative interesting approach to inversion formulas of the type of Equations 8.8 and 8.9 for the case when S is a sphere. It relies upon the idea of regarding the spherical mean operator as a member of a broader family of operators [76].

In 3D, if the sound speed is constant, the Huygens' principle applies, i.e., the pressure $p(t, x)$ inside S becomes equal to zero for any time T larger than the time required for sound to cross the domain. Thus, imposing zero conditions on $p(t, x)$ and $p_t(t, x)$ at $t=T$, and solving the wave Equation 8.2 back in time with the measured data g as the boundary values, one recovers at $t=0$ the source $f(x)$. This method, usually called **time reversal**, has been implemented in Ref. [77]. Although in even dimensions or in the presence of sound speed variations, Huygens' principle does not apply, one can find good approximate solutions by a similar approach [78]. Properties of the time reversal method and its comparison with other reconstruction methods of TAT are discussed in Ref. [78].

A different approach to TAT inversion is suggested in Ref. [79]. It is based on using not only the measured data g on $S \times \mathbb{R}^+$, but also the normal derivative of the pressure p on S. Since this normal derivative is not measured, finding it would require solving the exterior problem first and deriving the normal derivative from there. Feasibility and competitiveness of such a method for TAT is not clear at the moment.

8.9.3 Stability

Stability of inversion when S is a sphere surrounding the support of $f(x)$ is the same as for the standard Radon transform, as shown in the results of Refs. [9,26,74]. However, if the support reaches outside, in spite of Theorem 1 that guarantees uniqueness of reconstruction, stability for some parts of $f(x)$ lying outside S no longer holds (see Refs. [9,10,26,56] for details).

8.9.4 Range

The range conditions 2 and 3 of Theorem 4 are necessary also for nonspherical closed surfaces S and for functions with support outside S. They, however, are not expected to be sufficient, since the arising instabilities indicate that one might expect nonclosed ranges in some cases.

Some of the range conditions can be also described in the case of a variable sound speed [78].

ACKNOWLEDGMENTS

The work of the second author was partially supported by the NSF DMS grants 0604778 and 0648786. The third author was partially supported by the DOE grant DE-FG02-03ER25577 and NSF DMS grant 0312292. The work was partly done when the first two authors were visiting the Isaac Newton Institute for Mathematical Sciences (INI) in Cambridge. The authors express their gratitude to the NSF, DOE, and INI for this support. They also thank G. Ambartsoumian, G. Beylkin, D. Finch, A. Greenleaf, M. Klibanov, V. Palamodov, P. Stefanov, B. Vainberg, and E. Zuazua for information, and the reviewers and the editor for useful comments.

REFERENCES

1. Kruger, R.A., P. Liu, Y.R. Fang, and C.R. Appledorn. 1995. Photoacoustic ultrasound (PAUS) reconstruction tomography. *Med. Phys.* 22:1605–69.
2. Kruger, R.A., W.L. Kiser, D.R. Reinecke, and G.A. Kruger. 2003. Thermoacoustic computed tomography using a conventional linear transducer array. *Med. Phys.* 30(5):856–60.
3. Oraevsky, A.A., R.O. Esenaliev, S.L. Jacques, and F.K. Tittel. 1996. Laser optoacoustic tomography for medical diagnostics principles. *Proc. SPIE* 2676:22.
4. Oraevsky, A.A., and A.A. Karabutov. 2002. *Handbook of optical biomedical diagnostics*, Chapter 10, ed. V.V. Tuchin. Bellingham, WA: SPIE.
5. Oraevsky A.A., and A.A. Karabutov. 2003. Optoacoustic tomography. In *Biomedical photonics handbook*, ed. T. Vo-Dinh, 34/1–34/34. Boca Raton, FL: CRC.
6. Wang, X., Y. Pang, G. Ku, X. Xie, G. Stoica, and L.V. Wang. 2003. Noninvasive laser-induced photoacoustic tomography for structural and functional *in vivo* imaging of the brain. *Nat. Biotechnol.* 21(7):803–6.
7. Wang, L.V., and H. Wu. 2007. *Biomedical optics. Principles and imaging*. New York: Wiley-Interscience.
8. Xu, M., and L.-H.V. Wang. 2006. Photoacoustic imaging in biomedicine. *Rev. Sci. Instrum.* 77:041101–01–041101–22.
9. Kuchment, P., and L. Kunyansky. 2008. Mathematics of thermoacoustic tomography. *Eur. J. Appl. Math.* 19(2):191–224.
10. Louis, A.K., and E.T. Quinto. 2000. Local tomographic methods in Sonar. In *Surveys on solution methods for inverse problems*, eds. D. Colton, H. Engl, A. Louis, J. McLaughlin, and W. Rundell, 147–54. Vienna: Springer.
11. Nolan C.J., and M. Cheney. 2002. Synthetic aperture inversion. *Inverse Problems* 18:221–35.
12. Beylkin, G. 1984. The inversion problem and applications of the generalized Radon transform. *Comm. Pure Appl. Math.* 37:579–99.
13. Xu, M., and L.-H.V. Wang. 2002. Time-domain reconstruction for thermoacoustic tomography in a spherical geometry. *IEEE Trans. Med. Imaging* 21:814–22.
14. Agranovsky, M., and P. Kuchment. 2007. Uniqueness of reconstruction and an inversion procedure for thermoacoustic and photoacoustic tomography with variable sound speed. *Inverse Problems* 23:2089–102.
15. Jin, X., and L.V. Wang. 2006. Thermoacoustic tomography with correction for acoustic speed variations. *Phys. Med. Biol.* 51:6437–48.
16. Haltmeier, M., P. Burgholzer, G. Paltauf, and O. Scherzer. 2004. Thermoacoustic computed tomography with large planar receivers. *Inverse Problems* 20:1663–73.
17. Burgholzer, P., C. Hofer, G.J. Matt, G. Paltauf, M. Haltmeier, and O. Scherzer. 2006. Thermoacoustic tomography using a fiber-based Fabry-Perot interferometer as an integrating line detector. *Proc. SPIE* 6086:434–42.

18. Andersson, L.-E. 1988. On the determination of a function from spherical averages. *SIAM J. Math. Anal.* 19(1):214–32.
19. Fawcett, J.A. 1985. Inversion of n-dimensional spherical averages. *SIAM J. Appl. Math.* 45(2):336–41.
20. Natterer, F. and F. Wübbeling. 2001. *Mathematical methods in image reconstruction*. Monographs on Mathematical Modeling and Computation, v. 5. Philadelphia, PA: SIAM.
21. Xu, Y., D. Feng, and L.-H.V. Wang. 2002. Exact frequency-domain reconstruction for thermoacoustic tomography: I. Planar geometry. *IEEE Trans. Med. Imaging* 21:823–28.
22. Xu, Y., M. Xu, and L.-H.V. Wang. 2002. Exact frequency-domain reconstruction for thermoacoustic tomography: II. Cylindrical geometry. *IEEE Trans. Med. Imaging* 21:829–33.
23. Diebold, G.J., T. Sun, and M.I. Khan. 1991. Photoacoustic monopole radiation in one, two, and three dimensions. *Phys. Rev. Lett.* 67(24):3384–87.
24. Tam, A.C. 1986. Applications of photoacoustic sensing techniques. *Rev. Mod. Phys.* 58(2):381–431.
25. Agranovsky, M., C. Berenstein, and P. Kuchment. 1996. Approximation by spherical waves in L^p-spaces. *J. Geom. Anal.* 6(3):365–83.
26. Agranovsky, M., P. Kuchment, and E.T. Quinto. 2007. Range descriptions for the spherical mean Radon transform. *J. Funct. Anal.* 248:344–86.
27. Agranovsky M., and E.T. Quinto. 1996. Injectivity sets for the Radon transform over circles and complete systems of radial functions. *J. Funct. Anal.* 139:383–414.
28. Ambartsoumian G., and P. Kuchment. 2005. On the injectivity of the circular Radon transform. *Inverse Problems* 21:473–85.
29. Finch, D., S. Patch, and Rakesh. 2004. Determining a function from its mean values over a family of spheres. *SIAM J. Math. Anal.* 35(5):1213–40.
30. Courant R., and D. Hilbert. 1962. *Methods of mathematical physics, Volume II Partial differential equations.* New York: Interscience.
31. Finch, D., and Rakesh. 2008. Recovering a function from its spherical mean values in two and three dimensions. This volume.
32. Finch, D., and Rakesh. 2007. The spherical mean value operator with centers on a sphere. *Inverse Problems* 23(6):S37–S50.
33. Kuchment, P. 1993. Unpublished.
34. Kuchment, P. 2006. Generalized transforms of Radon type and their applications. *Proc. Symp. Appl. Math.,* American Math. Soc. 63:67–91.
35. Tataru, D. 1995. Unique continuation for solutions to PDEs; between Hörmander's theorem and Holmgren's theorem. *Comm. PDE* 20:814–22.
36. Norton, S.J. 1980. Reconstruction of a two-dimensional reflecting medium over a circular domain: Exact solution. *J. Acoust. Soc. Am.* 67:1266–73.
37. Norton, S.J., and M. Linzer. 1981. Ultrasonic reflectivity imaging in three dimensions: Exact inverse scattering solutions for plane, cylindrical, and spherical apertures. *IEEE Trans. Biomed. Eng.* 28:200–202.
38. Ehrenpreis, L. 2003. *The universality of the Radon transform*. New York: Oxford University Press.
39. Gelfand, I., S. Gindikin, and M. Graev. 2003. *Selected topics in integral geometry*, Transl. Math. Monogr. v. 220. Providence, RI: American Mathematical Society.
40. Helgason, S. 1980. *The Radon transform*. Basel: Birkhäuser.
41. Natterer, F. 1986. The mathematics of computerized tomography. New York: Wiley.
42. Popov, D.A., and D.V. Sushko. 2002. A parametrix for the problem of optical-acoustic tomography. *Dokl. Math.* 65(1):19–21.
43. Popov, D.A., and D.V. Sushko. 2004. Image restoration in optical-acoustic tomography. *Prob. Inform. Trans.* 40(3):254–78.
44. Xu, Y., L. Wang, G. Ambartsoumian, and P. Kuchment. 2004. Reconstructions in limited view thermoacoustic tomography. *Med. Phys.* 31(4):724–33.
45. Finch, D., M. Haltmeier, and Rakesh. 2007. Inversion of spherical means and the wave equation in even dimensions. *SIAM J. Appl. Math.* 68(2):392–412.
46. Kunyansky, L. 2007. Explicit inversion formulae for the spherical mean Radon transform. *Inverse Problems* 23:373–83.
47. Xu, M., and L.-H.V. Wang. 2005. Universal back-projection algorithm for photoacoustic computed tomography. *Phys. Rev. E* 71:016706.
48. Ambartsoumian, G., and S. Patch. 2007. Thermoacoustic tomography: Numerical results. *Proc. SPIE* 6437:64371B.
49. Oberhettinger, F. 1972. *Tables of Bessel transforms*. New York: Springer.
50. Kunyansky, L. 2007. A series solution and a fast algorithm for the inversion of the spherical mean Radon transform. *Inverse Problems* 23:S11–S20.
51. Vainberg, B. 1975. The short-wave asymptotic behavior of the solutions of stationary problems, and the asymptotic behavior as $t \to \infty$ of the solutions of nonstationary problems. *Russian Math. Surv.* 30(2):1–58.
52. Vainberg, B. 1989. *Asymptotics methods in the equations of mathematical physics*. London: Gordon and Breach. (Translation of the Russian 1982 edition.)
53. Egorov, Y.V., and M.A. Shubin. 1992. Linear Partial Differential Equations. Foundations of the Classical Theory. In *Partial differential equations. I.*, ed. Yu. V. Egorov and M. A. Shubin, Encyclopaedia of Mathematical Sciences, 30:1–259. Springer Verlag.
54. Xu, Y., L. Wang, G. Ambartsoumian, and P. Kuchment. 2008. Limited view thermoacoustic tomography. This volume.
55. Kuchment, P., and E.T. Quinto. 2003. Some problems of integral geometry arising in tomography Appendix. In *The universality of the Radon transform*, by L. Ehrenpreis. New York: Oxford University Press.
56. Quinto, E.T. 1993. Singularities of the X-ray transform and limited data tomography in $\mathbb{R}^2$ and $\mathbb{R}^3$. *SIAM J. Math. Anal.* 24:1215–25.
57. Palamodov, V.P. 2004. *Reconstructive integral geometry*. Basel: Birkhäuser.
58. Gelfand, I., S. Gindikin, and M. Graev. 1980. Integral geometry in affine and projective spaces. *J. Sov. Math.* 18:39–167.
59. Gelfand, I., M. Graev, and N. Vilenkin. 1965. *Generalized functions, v. 5: Integral geometry and representation theory*. New York: Academic Press.
60. Helgason, S. 2000. *Groups and geometric analysis*. Providence, RI: American Mathematical Society.
61. Kuchment, P., and S. Lvin. 1990. Paley-Wiener theorem for the exponential Radon transform. *Acta Appl. Math.* 18:251–60.
62. Kuchment, P., and S. Lvin. 1991. The range of the exponential Radon transform. *Soviet Math. Dokl.* 42(1):83–184.
63. Lvin, S. 1994. Data correction and restoration in emission tomography. In *Tomography, impedance imaging, and integral geometry*, ed. E.T. Quinto, M. Cheney, and P. Kuchment, 149–155, Lectures in Applied Mathematics, Vol. 30. Providence, RI: American Mathematical Society.
64. Novikov, R. 2002. On the range characterization for the two-dimensional attenuated X-ray transform. *Inverse Problems* 18:677–700.
65. Ponomarev, I. 1995. Correction of emission tomography data. Effects of detector displacement and non-constant sensitivity. *Inverse Problems* 10:1–8.

66. Lin, V., and A. Pinkus. 1993. Fundamentality of ridge functions. *J. Approx. Theory* 75:295–311.
67. Lin, V., and A. Pinkus. 1994. Approximation of multivariate functions In *Advances in computational mathematics*, ed. H. P. Dikshit and C. A. Micchelli, 1–9. River Edge, NJ: World Science Publications.
68. Bouzaglo-Burov, E. 2005. Inversion of spherical Radon transform, methods and numerical experiments. [In Hebrew.] MS thesis, Bar-Ilan University.
69. Patch, S.K. 2004. Thermoacoustic tomography–consistency conditions and the partial scan problem. *Phys. Med. Biol.* 49:1–11.
70. Ambartsoumian, G., and P. Kuchment. 2006. A range description for the planar circular Radon transform. *SIAM J. Math. Anal.* 38(2):681–92.
71. Finch, D., and Rakesh. 2006. The range of the spherical mean value operator for functions supported in a ball. *Inverse Problems* 22:923–38.
72. Asgeirsson, L. 1937. Über eine Mittelwerteigenschaft von Lösungenhomogenerlinearerpartiellerdifferentialgleichungen zweiter Ordnung mit konstanten Koeffizienten. *Ann. Math.* 113:321–46.
73. John, F. 1971. *Plane waves and spherical means, applied to partial differential equations*. Mineola, NY: Dover.
74. Palamodov, V. 2007. Remarks on the general Funk-Radon transform and thermoacoustic tomography. Preprint, arXiv: math/0701204.
75. Gindikin, S. 1995. Integral geometry on real quadrics. In *Lie groups and lie algebras: E.B. Dynkin's seminar*, 23–31, Am. Math. Soc. Transl. Ser. 2, 169. Providence, RI: American Mathematical Society.
76. Rubin, B. 2007. Spherical means in odd dimensions and EPD equations. Preprint arXiv:0711.1897.
77. Burgholzer, P., G. Matt, M. Haltmeier, and G. Patlauf. 2007. Exact and approximate imaging methods for photoacoustic tomography using an arbitrary detection surface. *Phys. Rev. E* 75:046706.
78. Hristova, Y., P. Kuchment, and L.V. Nguyen. 2008. On reconstruction and time reversal in thermoacoustic tomography in acoustically homogeneous and inhomogeneous media. *Inverse Problems* 24:055006.
79. Clason, C., and M. Klibanov. 2007. The quasi-reversibility method in thermoacoustic tomography in a heterogeneous medium. *SIAM J. Sci. Comp.* 30:1–23.
80. Olafsson, G., and E.T. Quinto, eds. 2006. The Radon transform, inverse problems, and tomography. American Mathematical Society Short Course January 3–4, 2005, Atlanta, Georgia, Proc. Symp. Appl. Math., v. 63. Providence, RI: American Mathematical Society.